Journal of Nuclear Medicine, published on June 6, 2019 as doi:10.2967/jnumed.119.225870

The characterization of 18F-hGTS13 for molecular imaging of x_C^- transporter activity with positron emission tomography

Corinne Beinat[1], Gayatri Gowrishankar[1], Bin Shen[1], Israt S. Alam[1], Elise Robinson[1], Tom Haywood[1], Chirag B. Patel[1,2], Emily Carmen Azevedo[1], Jessa B. Castillo[1], Ohad Ilovich[1], Norman Koglin[3], Heribert Schmitt-Willich[3], Mathias Berndt[3], Andre Mueller[3], Marion Zerna[3], Ananth Srinivasan[1], and Sanjiv Sam Gambhir[1,4]*

[1]Department of Radiology, Molecular Imaging Program at Stanford (MIPS), Stanford University School of Medicine, Stanford, CA, 94305, USA

[2]Department of Neurology and Neurological Sciences, Stanford University School of Medicine, Stanford, CA, 94305, USA

[3]Life Molecular Imaging GmbH (formerly Piramal Imaging) GmbH, Berlin, Tegeler Strasse 6-7, 13353 Berlin, Germany

[4]Departments of Bioengineering and Materials Science & Engineering, Bio-X, Stanford University, Stanford, CA 943065, USA.

Correspondence to: Sanjiv Sam Gambhir; 318 Campus Drive, E153, Stanford, CA, 94305; phone: (650) 725-6175; fax: (650) 724-4948; email: sgambhir@stanford.edu

First author contact details: Corinne Beinat; 318 Campus Drive E150, Stanford, CA, 94305; phone: (650)-725-3113; fax: (650) 724-4948; email: cbeinat@stanford.edu

Running title: Characterization of 18F-hGTS13

Keywords: x_C^- transporter, oxidative stress, cancer metabolism, PET imaging, 18F-hGTS13

Disclosure: This work was partly supported by Life Molecular Imaging GmbH (formerly Piramal Imaging).

Number of figures: 6

ABSTRACT

Purpose: The aim of this study was development of an improved positron emission tomography (PET) radiotracer for measuring x_C^- activity with increased tumor uptake and reduced uptake in inflammatory cells compared to (*S*)-4-(3-18F-Fluoropropyl)-L-glutamic acid (18F-FSPG).

Experimental design: A racemic glutamate derivative, 18F-hGTS13 was evaluated in cell culture and animal tumor models. 18F-hGTS13 was separated into C5-epimers and the corresponding 18F-hGTS13-isomer1 and 18F-hGTS13-isomer2 evaluated in H460 tumor bearing rats. Preliminary studies investigate the cellular uptake of 18F-hGTS13-isomer2 in multiple immune cell populations and states.

Results: 18F-hGTS13 demonstrated excellent H460 tumor visualization with high tumor-to-background ratios, confirmed by ex vivo biodistribution studies. Tumor associated radioactivity of 18F-hGTS13 (7.5±0.9%ID/g, n=3) was significantly higher than with 18F-FSPG (4.6±0.7%ID/g, n=3, p=0.01). 18F-hGTS13-isomer2 exhibited excellent H460 tumor visualization (6.3±1.1%ID/g, n-3), and significantly reduced uptake in multiple immune cell populations relative to 18F-FSPG. 18F-hGTS13-isomer2 exhibited increased liver uptake relative to 18F-FSPG (4.6±0.8%ID/g vs. 0.7±0.01%ID/g) limiting its application in hepatocellular carcinoma.

Conclusion: 18F-hGTS13-isomer2 is a new PET radiotracer for molecular imaging of x_C^- activity which may provide information regarding tumor oxidation states. 18F-hGTS13-isomer2 has potential for clinical translation for imaging cancers of the thorax due to the low background signal in healthy tissue.

INTRODUCTION

The increased uptake of glucose has been exploited clinically to detect tumors and their response to treatment by positron emission tomography (PET) imaging with 2-18F-fluoro-2-deoxyglucose (18F-FDG) (*1,2*). However, 18F-FDG has limitations including non-specificity towards inflammation, and high background accumulation in tissues with high glycolytic rates including brain and heart (*3*). To overcome limitations of 18F-FDG and provide additional information about tumor biology, other fundamental processes in tumor cells would be of utility for cancer detection, monitoring treatment response and predicting chemoresistance (*4*). The enhanced rate of glucose and glutamine uptake to increase cell mass results in elevated levels of oxidative intermediates and subsequent altered redox potential and excess of reactive oxygen species (*5*). Thiol containing molecules, including L-cysteine and the tripeptide glutathione (GSH) are key cellular components to neutralize these conditions and their consumption leads to detoxification of reactive oxygen species and other electrophiles (e.g., chemotherapeutics) (*6*). GSH is the major thiol-containing endogenous antioxidant, found in millimolar intracellular concentrations and serves as a redox buffer against various sources of oxidative stress (*7-9*). A constant supply of GSH and its precursory components are essential for cell survival and provide an advantage for tumor growth. L-cysteine plays a crucial role as a reactive oxygen species scavenger and is also the rate limiting constituent in GSH biosynthesis (*10*). L-cysteine is provided to cells via system x_C^-, the amino acid transporter that mediates the sodium independent exchange of extracellular L-cystine and intracellular L-glutamate across the plasma membrane (*11*) (Fig. 1). Intracellularly, L-cystine is reduced to two molecules of L-cysteine which can be utilized for GSH biosynthesis. System x_C^- is a heterodimeric transporter consisting of two subunits; the light chain x_CT (SLC7A11) conferring substrate specificity, and the heavy chain 4F2hc (SLC3A2) (*12*). It is noteworthy that x_C^- is unable

to differentiate between its natural substrates L-Cystine and L-Glutamate for the inward direction of transport (*13*). The increased activity of x_C^- in tumors has previously been exploited by PET imaging with (4*S*-4-(3-18F-fluoropropyl)-L-glutamate (18F-FSPG). Pilot clinical studies have been completed examining dosimetry in healthy volunteers, and tumor detection in non-small cell lung carcinoma, breast cancer (*14*), hepatocellular cancer (*15*), and intracranial malignancies (*16*). Additional radiotracers including 18F-5-fluoro-aminosuberic acid (18F-FASu) targeting the x_C^- transporter have also been described (*17,18*). As the x_C^- transporter plays important roles in other non-tumor related diseases, 18F-FSPG has high uptake and retention in inflammatory cells (*19*) including activated T cells and microglia, resulting in the investigation of 18F-FSPG to visualize multiple sclerosis (*20*), and cerebral ischemia (*21*). With these considerations in mind, second generation radiotracers for molecular imaging of x_C^- were designed (WO/2012/150220), with potential for reduced uptake in inflammatory cells and enhanced tumor visualization. Incorporation of an ultraviolet active moiety was pursued to facilitate radiosynthesis and quality control as 18F-FSPG requires derivitization for quality control analysis at our institution. The compound hGTS13 was selected for further evaluation.

MATERIALS AND METHODS

General

Human A549 and H460 tumor cell lines were obtained from ATCC (Manassas, VA) and maintained according to the provider's protocols. Chemicals were obtained from Sigma-Aldrich (St. Louis, MO), Tocris (Bristol, United Kingdom) and Thermo Fisher-Scientific (Waltham, MA). Synthesis of the precursor, tosylate di-*tert*-butyl (2*S*)-2-[(*tert*-butoxycarbonyl)amino]-5-{4-[2-(tosyloxy)ethoxy]benzylhexanedioate (compound 1) was adopted from a patent (WO/2012/150220). 18F-FSPG was obtained from Stanford Cyclotron and Radiochemistry Facility.

Radiochemistry

18F-hGTS13 was synthesized from nucleophilic displacement of the tosylate group within compound 1 and subsequent de-protection (Supplemental Fig 1), full details can be found in Supplemental Material. The identity of 18F-hGTS13 was confirmed through co-injection with reference standard 19F-hGTS13 (Supplemental Figure 2).

Chiral High Performance Liquid Chromatography

C5 epimers of compound 1 were separated by high performance liquid chromatography using a chiral column (Lux® 5 µM Amylose-1, 150 × 4.6 mm). An isocratic mobile phase of hexane/isopropanol (85:10) + 0.1% diethylamine was used (flow rate 1.0 mL/min) to give baseline separation of C5 epimers, Rt 6.4 and 8.5 mins.

Cell Uptake Studies

A549 and H460 cells (2 x 10^5) were plated into twelve-well plates the day before uptake studies (n=3 per condition). On the day of the uptake, pre-warmed Hanks balanced salt solution (HBSS) containing ~0.2 MBq of 18F-hGTS13 was added to individual wells (1 mL per well). Cells were incubated at 37 °C and 5% CO_2 over a specified time course. For competition studies, wells were pre-treated 10 min prior to radiotracer addition with the appropriate amino acid or (*S*)-4-carboxyphenylglycine to give a final concentration of 1 mM (n=3 replicates per inhibitor). HBSS containing the inhibitors was aspirated and fresh HBSS containing the appropriate inhibitor and 0.2 MBq of 18F-hGTS13 added and incubated 37°C and 5% CO_2 for 60 min. Cells were processed as previously described (*22*).

x_CT siRNA

A549 cells (6×10^4) were seeded in 12-well plates in antibiotic-free F-12K media the day before addition of siRNA transfection with Lipofectamine 2000 according to the manufacturer's instructions. Specific siRNA sequences targeting the light chain x_CT were produced by Thermo Scientific using the following sequence: CGAGTCTGGGTGGAACTCCTCATAA. Scrambled siRNA (CGAGGTCGGTGTCAACTCCATGTAA) was used as a control. siRNA was added at a final concentration of 25nM and x_CT knockdown achieved 48 hours after transfection, confirmed through qRT-PCR and 14C-cystine uptake studies. 18F-hGTS13 uptake was measured over 60 min in cells treated with x_CT siRNA and control siRNA at 48 hours after transfection. Cells were processed for tracer uptake studies as described above using 18F-hGTS13 or 14C-cystine. For 14C-cystine measurements, 10 mL of scintillation liquid was added to lysates, and measured using

an LS 6500 Multi-purpose scintillation counter (Beckman Coulter, Pasadena, CA). Untreated cells were used as an additional control, measured 72 hours after seeding.

RNA Isolation, Reverse Transcription and qRT-PCR

Total RNA was extracted with an RNeasy mini kit (Qiagen, Hilden, Germany). cDNA was synthesized with M-MLV Reverse Transcriptase (Thermo Fisher Scientific) using oligo(dT) primers according to the manufacturer's protocol. Real-time PCR was performed on the iCycler Real-Time PCR Detection System (Bio-Rad, Hercules, CA) using SYBR Green PCR Master Mix (Life Technologies, Carlsbad, CA) with primers specific for x_CT and 18S rRNA using annealing and extension temperatures of 56 ºC and 72 ºC respectively. x_CT was amplified using primers (forward) 5′-CAAATGCAGTGGCAGTGACC and (reverse) 5′-AGACAGCAAACACACCACCG, and 18S rRNA was amplified using (forward) 5′-GTAACCCGTTGAACCCCATT and (reverse) 5′-CCATCCAATCGGTAGTAGCG primers. Transcript levels were normalized to the level of 18S rRNA mRNA. The comparative quantitation method (ΔΔCt) was used to compare the different samples and transform them to absolute values with $2^{-\Delta\Delta Ct}$ for determining relative fold changes.

Primary Human Immune Cell Isolation, Activation and Radiotracer Uptake Studies

Human peripheral blood mononuclear cells (PBMCs) were obtained from fresh buffy coat fractions (Stanford Blood Center) using Ficoll-Paque Plus following the manufacturer's instructions (GE Healthcare, Chicago, IL). T cells, B cells and monocytes were isolated using the Human Naïve Pan T Cell Isolation kit, Human B Cell Enrichment kit and Human Monocyte

Isolation kit respectively (Stemcell Technologies, Vancouver, Canada). Isolated cells were subsequently maintained in resting or activated conditions for 2 days. T cells were activated with the T cell activation/expansion kit using anti-CD3/2/28 coated particles (Miltenyi Biotec, Auburn, CA). B cells were activated with CpG Oligodeoxynucleotide 2006 (1 μM; Sigma-Aldrich). Monocytes were activated using Lipopolysaccharide (1 μg/mL; Escherichia coli O55:B5; Sigma-Aldrich) (*23-25*). Activation was confirmed by assessing significant changes in morphology in activated versus resting cells.

Radiotracer uptake experiments were performed 48 hours after activation. Cells from the same donor were used to evaluate uptake of both 18F-hGTS13-isomer2 and 18F-FSPG to minimize donor dependent variation. T cells, B cells and monocytes (3×10^5 per well) were prepared in pre-warmed HBSS in a 96 well plate and incubated with ~0.8 MBq of radiotracer per well for 1 hour. Cells were processed as previously described (*26*).

Animal Studies

All experiments involving animals were in accordance with protocols approved by the Institutional Animal Care and Use Committee at Stanford University and were performed based on the NIH Guide for the Care and Use of Laboratory Animals. H460 subcutaneous tumor models were developed as previously described (*27*). PET/CT imaging of rats was performed with a small animal hybrid scanner (Inveon, Siemens) and analyzed according to methods previously described by our group (*22*). Approximately 15 MBq (400 μCi) of each radiotracer was administered to rats intravenously. For comparative radiotracer studies the same cohort of rats was scanned with each radiotracer, representative images show comparison within the same animal. Static PET scans

were acquired 60 mins after injection of radioactivity, the acquisition of dynamic PET scans commenced immediately before injection of radiotracer. No partial volume correction was completed.

Ex Vivo Biodistribution Studies

At completion of PET imaging studies, ~80 minutes after radiotracer administration, rats were sacrificed by terminal cardiac puncture and tissues harvested. Radioactivity within individual tissues was determined on a gamma counter. Radioactivity standards were counted for data normalization. Data were expressed as %ID/g.

Statistical Analyses

Data were expressed as mean ± standard deviation. Statistical significance was determined using a two-tailed Student's t test, p-value <0.05 was determined significant. For analysis across multiple samples, 1 or 2-way analysis of variance (ANOVA) was used followed by multiple comparisons of means with Bonferroni correction

RESULTS

18F-hGTS13 Shows Rapid and Extensive Uptake in Cell Culture

Cell culture studies showed rapid cellular uptake in A549 and H460 tumor cells post addition of 18F-hGTS13, with uptake values of 9.7 ± 2.8% and 21.6 ± 3.6% at 30 and 60 min respectively in A549 cells and 15.8 ± 1.5% and 32.1 ± 0.8% in H460 cells (Fig. 2A). Strong

inhibition of 18F-hGTS13 uptake was evident in the presence of L-Glutamate, L-Cystine or the system x_C^- specific inhibitor p-carboxyphenylglycine (CPG). However, no inhibition of uptake was evident in the presence of L-Aspartate. The competition profile of 18F-hGTS13 in both A549 and H460 cells is highlighted in Fig. 2B and indicates the specificity of this radiotracer for system x_C^-. We additionally modulated light chain x_CT protein expression *in vitro* through small inhibitory RNA (siRNA), reduced x_CT expression was confirmed through PCR and 14C-cystine uptake (Supplemental Fig. 3). A significant reduction in 18F-hGTS13 uptake (78%, $p<0.0001$, n=3 per condition) was evident in x_CT siRNA cells compared to those transfected with control siNRA (Fig. 2C). Competition studies in the presence of L-Glutamine, L-Leucine and L-Alanine suggest possible involvement of Systems L and B^{+0} in the uptake of 18F-hGTS13, particularly in A549 cells (Supplemental Fig. 4), while additional knockdown studies (Fig. 2C and Supplemental Fig. 5) indicate specificity to system x_C^- and a similar specificity profile to 18F-FSPG.

Evaluation of 18F-hGTS13 in H460 Tumor-Bearing Rats

In xenograft models of H460 cells, 10 min static PET/CT imaging were completed 60 min after injection of 18F-hGTS13. The distribution of 18F-hGTS13 was characterized by renal clearance as well as liver uptake (Fig. 3). High tumor uptake (7.5±0.9 %ID/g) was evident at 60 min post injection of radioactivity. Rats bearing H460 tumors were additionally scanned one day prior with 18F-FSPG PET/CT, levels of radioactivity within H460 tumors were significantly lower with 18F-FSPG compared to 18F-hGTS13 (4.6±0.7, $p=0.01$, n=3). *Ex vivo* biodistribution studies following the 18F-hGTS13 PET scan corroborated the PET imaging results (Fig. 3C), 18F-hGTS13 radioactivity in the H460 tumor was determined to be 6.4±0.9 %ID/g, which was

significantly higher than that of blood (0.6±0.2 %ID/g, p=0.0042, n=3) and muscle (0.1±0.05 %ID/g, p=0.0004, n=3).

Separation of 18F-hGTS13 C-5 Epimers and Evaluation in H460 Tumor Bearing Rats

Chiral high performance liquid chromatography of compound 1 gave baseline separation of C-5 epimers with Rt of 6.4 and 8.5 min. No efforts were made to resolve the absolute stereochemistry of the isomers at this stage, they were defined as isomer 1 and isomer 2 based on order of elution from the chiral column. Radiolabeling of the C-5 epimers of compound 1 to give 18F-hGTS13-isomer1 and 18F-hGTS13-isomer2 was achieved utilizing the method described for the racemic mixture. 18F-hGTS13-isomer1 and 18F-hGTS13-isomer2 were synthesized respectively in 4.4% (n=1) and 5.1 ± 1.7% (n=2) radiochemical yield, non-decay corrected. H460 tumor bearing rats were evaluated with static PET/CT imaging of 18F-hGTS13-isomer1 and 18F-hGTS13-isomer2 (4 days apart) (Fig. 4). A significant reduction in liver uptake was observed with 18F-hGTS13-isomer2 compared to 18F-hGTS13-isomer1 at 60 min post injection of radioactivity (4.7±0.9 %ID/g vs 8.5±0.4 %ID/g, p=0.01, n=3). There were similar amounts of radioactivity retained in H460 tumors between 18F-hGTS13-isomer1 and 18F-hGTS13-isomer2 (6.7±1.1 %ID/g vs 6.3±1.6 %ID/g, p=0.8, n=3). Further studies were completed with 18F-hGTS13-isomer2 based on the improved biodistribution profile and similar levels of radioactivity retained in H460 tumors. Dynamic PET/CT imaging with 18F-hGTS13-isomer2 was completed over a 60 min time period (Fig. 5). High H460 tumor accumulation was evident throughout the scan with radiotracer uptake values continuing to rise over the 60 min period (4.7 ± 1.3 %ID/g at 60 min post injection), suggesting peak tumor radiotracer uptake may occur beyond the 60 min acquisition period. Levels of radioactivity present in healthy lung tissue and muscle were low throughout the scan,

highlighting the potential for high tumor-to-background in cancers of the thorax (Supplemental Fig. 6A). Results of the PET imaging studied were confirmed through *ex vivo* biodistribution (Supplemental Fig. 6B).

Evaluation of 18F-hGTS13-isomer2 in Immune Cell Populations Compared to 18F-FSPG

We evaluated the uptake of 18F-hGTS13-isomer2 compared to 18F-FSPG in primary human T cells, B cells and monocytes; key immune cell populations in various inflammatory diseases and the tumor microenvironment. These studies revealed a dramatic increase in the uptake of 18F-FSPG in activated versus resting T cells (72-fold, $p<0.0001$, n=3) (Fig. 6A) consistent with previous studies (*26*). In contrast, the increased uptake of 18F-hGTS13-isomer2 in activated T cells was attenuated; 17-fold increase relative to resting T cells ($p=0.0002$, n=3). A similar trend was observed with B cells where 18F-FSPG exhibited a 3-fold increased uptake in activated versus resting B cells ($p=0.0003$, n=3, Figure 6B). In contrast, 18F-hGTS13-isomer2 displayed a 2-fold increase in uptake in activated versus resting B cells ($p=0.189$, n=3). Finally in monocytes, 18F-FSPG displayed a 2-fold increase uptake in activated versus resting monocytes ($p=0.0022$, n=3) whereas 18F-hGTS13-isomer2 exhibited a 4-fold increased uptake in activated versus resting monocytes ($p<0.0001$, n=3, Figure 6C), however 18F-hGTS13-isomer2 absolute uptake values were considerably lower.

DISCUSSION

System x_C^- represents an attractive target for PET imaging due to its involvement in mediating cellular response to oxidative stress and detoxification processes which support tumor

progression and therapy resistance. Molecular imaging of x_C^- activity provides additional information over other amino acid based PET probes currently being explored including 18F-FET and 18F-FDOPA, which are taken up primarily by L-type amino acid transporter (LAT) mechanisms and largely reflect nutrient uptake to support increased biomass and proliferative energy demands (*28*). The present work describes the characterization of a novel radiotracer, 18F-hGTS13-isomer2, for PET imaging of x_C^- activity and evaluation in cell culture and preclinical models.

The capacity of cancer cells to achieve multidrug resistance remains an obstacle for successful chemotherapy, x_C^- plays a vital role in the development of multidrug resistance in cancer. Increased x_C^- expression is associated with chemoresistance of tumor cells; a negative correlation is evident between its expression and drug potency across NCI-60 cancer cell lines (*29*). A negative correlation is similarly evident between x_C^- expression and the anti-cancer activity of compounds which contain structural features amenable to GSH reactivity, including Mannich base, therefore indicating that GSH-dependent inactivation is a potential mechanism through which x_C^- expression induces chemoresistance (*30*). Molecular imaging of x_C^- activity provides the potential to visualize this important target in oncology and gain insight into the mechanisms of cancer drug resistance. PET imaging of x_C^- activity with 18F-hGTS13-isomer2 may provide the potential to visualize tumors and provide valuable insight into chemoresistance, particularly in cancers of the thorax due to the low background signal in healthy tissue. Although 18F-hGTS13-isomer2 displayed a favorable increase in tumor uptake, an increase in radiotracer uptake was also evident in the liver compared to 18F-FSPG, potentially limiting the ability of this radiotracer for imaging hepatocellular cancer, where 18F-FSPG has shown utility (*31*). There are no anticipated

concerns in radiation dosimetry based on the increased liver uptake. Key applications where 18F-hGTS13-isomer2 may have advantages over 18F-FSPG include lung cancer, breast cancer and primary and metastatic brain lesions.

Several lines of evidence suggest the role of x_C^- in regulating the innate and adaptive immune response. Activation of monocytes is associated with production of reactive oxygen species, the x_C^- is subsequently upregulated potentially as an auto-protective response during activation of these cells (*32*). Similarly, naïve T cells are known to be metabolically dependent on antigen presenting cells to fulfil their cysteine requirements due to the lack of x_C^- and limited cysteine availability in the extracellular space. However, upon activation of T cells, expression of x_C^- becomes upregulated and provides activated T cells with cysteine necessary for proliferation (*33,34*). Aside from malignant cells, the tumor microenvironment contains a complex milieu of immune cells including T- and B-lymphocytes, tumor-associated macrophages and monocytes, as well as fibroblasts and vascular endothelial cells (*35*). The x_C^- expression and uptake of 18F-FSPG in several of these cell populations has been previously investigated (*26,33,36*), although 18F-hGTS13-isomer2 uptake was elevated in activated vs. resting immune cells, the differential observed between activated and resting cells as well as the absolute levels of uptake was much lower than observed with 18F-FSPG. Although both compounds are specifically taken up through the same transporter, structural differences (length of the carbon-backbone and the side-chain) may cause more directed inward-channeling of one compound over the other depending on the context of the transporter activity, i.e. cancer or inflammation, and associated driving forces. Future studies including immune cell blocking studies will be required to evaluate this in detail. Additional studies including *in vivo* inflammation models will be required to determine if these findings

persist in animal models. Nevertheless, the results of 18F-hGTS13-isomer2 in cell culture and in animal models are promising and highlight the potential of this radiotracer, with improved specificity for imaging cancer cells in the tumor microenvironment.

CONCLUSION

18F-hGTS13-isomer2 is a new radiotracer for molecular imaging of x_C^- activity, specifically taken up by x_C^- in cell culture and with high tumor accumulation in animal models. Molecular imaging of x_C^- activity with 18F-hGTS13-isomer2 has potential for improved tumor detection and staging compared to other x_C^- targeting radiotracers and may assist in directing therapeutic strategies by visualizing metabolic adaptations to oxidative stress. Future studies are required to elucidate the uptake of 18F-hGTS13-isomer2 in inflammation states *in vivo* and to associate radiotracer uptake with chemoresistance. Clinical translation of 18F-hGTS13-isomer2 is underway for molecular imaging of cancers of the thorax.

DISCLOSURE

This work was partly supported by Life Molecular Imaging GmbH (formerly Piramal Imaging). No other potential conflict of interest relevant to this article was reported.

ACKNOWLEDGEMENTS

We thank the Radiochemistry Facility and Small Animal Imaging Facility at Stanford University. CB acknowledges receipt of a Stanford Translational Research and Applied Medicine

Fellowship. The authors acknowledge support from Thomas Brumby, Georg Kettschau and Timo Stellfeld of Bayer Pharma (Berlin, Germany) in the development of this compound.

KEY POINTS: The goal of this study was development of a novel radiotracer for molecular imaging of x_C^- activity with improved tumor uptake and reduced uptake in inflammatory cells. 18F-hGTS13-isomer2 exhibited excellent H460 tumor visualization, and significantly reduced uptake in multiple immune cell populations. 18F-hGTS13-isomer2 has potential for clinical translation for imaging cancers of the thorax due to the low background signal in healthy tissue.

REFERENCES:

1. Kelloff GJ, Hoffman JM, Johnson B, et al. Progress and promise of FDG-PET imaging for cancer patient management and oncologic drug development. *Clin Cancer Res.* 2005;11:2785-2808.

2. Pantel AR, Ackerman D, Lee SC, Mankoff DA, Gade TP. Imaging cancer metabolism: Underlying biology and emerging strategies. *J Nucl Med.* 2018;59:1340-1349.

3. Shreve PD, Anzai Y, Wahl RL. Pitfalls in oncologic diagnosis with FDG PET imaging: Physiologic and benign variants. *Radiographics.* 1999;19:61-77; quiz 150-151.

4. Mankoff DA, Eary JF, Link JM, et al. Tumor-specific positron emission tomography imaging in patients: [18F] fluorodeoxyglucose and beyond. *Clin Cancer Res.* 2007;13:3460-3469.

5. Levine AJ, Puzio-Kuter AM. The control of the metabolic switch in cancers by oncogenes and tumor suppressor genes. *Science.* 2010;330:1340-1344.

6. Okuno S, Sato H, Kuriyama-Matsumura K, et al. Role of cystine transport in intracellular glutathione level and cisplatin resistance in human ovarian cancer cell lines. *Br J Cancer.* 2003;88:951-956.

7. Meister A. Glutathione metabolism. *Methods Enzymol.* 1995;251:3-7.

8. DeBerardinis RJ, Cheng T. Q's next: The diverse functions of glutamine in metabolism, cell biology and cancer. *Oncogene.* 2010;29:313-324.

9. Estrela JM, Ortega A, Obrador E. Glutathione in cancer biology and therapy. *Crit Rev Clin Lab Sci.* 2006;43:143-181.

10. Lu SC. Glutathione synthesis. *Biochim Biophys Acta.* 2013;1830:3143-3153.

11. Bridges RJ NN, Patel SA. System xc- cystine/glutamate antiporter: An update on molecular pharmacology and roles within the cns. *Br J Pharmacol.* 2012;165:20-34.

12. Bassi MT, Gasol E, Manzoni M, et al. Identification and characterisation of human xct that co-expresses, with 4f2 heavy chain, the amino acid transport activity system xc. *Pflugers Arch.* 2001;442:286-296.

13. Patel SA, Warren BA, Rhoderick JF, Bridges RJ. Differentiation of substrate and non-substrate inhibitors of transport system xc(-): An obligate exchanger of l-glutamate and l-cystine. *Neuropharmacology.* 2004;46:273-284.

14. Baek S, Choi CM, Ahn SH, et al. Exploratory clinical trial of (4s)-4-(3-[18F]fluoropropyl)-l-glutamate for imaging xc- transporter using positron emission tomography in patients with non-small cell lung or breast cancer. *Clin Cancer Res.* 2012;18:5427-5437.

15. Baek S, Mueller A, Lim Y-S, et al. (4s)-4-(3-18f-fluoropropyl)-l-glutamate for imaging of xc^- transporter activity in hepatocellular carcinoma using pet: Preclinical and exploratory clinical studies. *J Nucl Med.* 2013;54:117-123.

16. Mittra ES, Koglin N, Mosci C, et al. Pilot preclinical and clinical evaluation of (4S)-4-(3-[18F]fluoropropyl)-l-glutamate (18F-FSPG) for PET/CT imaging of intracranial malignancies.

PLoS One. 2016;11:e0148628.

17. Webster JM, Morton CA, Johnson BF, et al. Functional imaging of oxidative stress with a novel pet imaging agent, 18F-5-fluoro-l-aminosuberic acid. *J Nucl Med.* 2014;55:657-664.

18. Yang H, Jenni S, Colovic M, et al. (18)F-5-fluoroaminosuberic acid as a potential tracer to gauge oxidative stress in breast cancer models. *J Nucl Med.* 2017;58:367-373.

19. Chae SY, Choi CM, Shim TS, et al. Exploratory clinical investigation of (4S)-4-(3-18F-fluoropropyl)-l-glutamate pet of inflammatory and infectious lesions. *J Nucl Med.* 2016;57:67-69.

20. Martín A, Vázquez-Villoldo N, Gómez-Vallejo V, et al. In vivo imaging of system xc- as a novel approach to monitor multiple sclerosis. *Eur J Nucl Med Mol Imaging.* 2016;43:1124-1138.

21. Domercq M, Szczupak B, Gejo J, et al. Pet imaging with [(18)F]FSPG evidences the role of system xc(-) on brain inflammation following cerebral ischemia in rats. *Theranostics.* 2016;6:1753-1767.

22. Beinat C, Haywood T, Chen YS, et al. The utility of [(18)F]DASA-23 for molecular imaging of prostate cancer with positron emission tomography. *Mol Imaging Biol.* 2018;20:1015-1024.

23. Krieg AM, Yi A-K, Matson S, et al. Cpg motifs in bacterial DNA trigger direct b-cell activation. *Nature.* 1995;374:546-549.

24. Trickett A, Kwan YL. T cell stimulation and expansion using anti-cd3/cd28 beads. *J Immunol Methods.* 2003;275:251-255.

25. Plevin RE, Knoll M, McKay M, Arbabi S, Cuschieri J. The role of lipopolysaccharide structure in monocyte activation and cytokine secretion. *Shock* 2016;45:22-27.

26. Hoehne A, James ML, Alam IS, et al. [(18)F]FSPG-PET reveals increased cystine/glutamate antiporter (xc-) activity in a mouse model of multiple sclerosis. *J Neuroinflammation.* 2018;15:55.

27. Koglin N, Mueller A, Berndt M, et al. Specific pet imaging of xc transporter activity using a 18F-labeled glutamate derivative reveals a dominant pathway in tumor metabolism. *Clin Cancer Res.* 2011;17:6000-6011.

28. Sun A, Liu X, Tang G. Carbon-11 and fluorine-18 labeled amino acid tracers for positron emission tomography imaging of tumors. *Front Chem.* 2018;5:124-124.

29. Huang Y, Dai Z, Barbacioru C, Sadée W. Cystine-glutamate transporter slc7a11; in cancer chemosensitivity and chemoresistance. *Cancer Res.* 2005;65:7446.

30. Dai Z, Huang Y, Sadee W, Blower P. Chemoinformatics analysis identifies cytotoxic compounds susceptible to chemoresistance mediated by glutathione and cystine/glutamate transport system xc. *J Med Chem.* 2007;50:1896-1906.

31. Kavanaugh G, Williams J, Morris AS, et al. Utility of [(18)F]FSPG PET to image hepatocellular carcinoma: First clinical evaluation in a us population. *Mol Imaging Biol.* 2016;18:924-934.

32. Pampliega O, Domercq M, Soria FN, Villoslada P, Rodríguez-Antigüedad A, Matute C. Increased expression of cystine/glutamate antiporter in multiple sclerosis. *J Neuroinflammation.* 2011;8:63-63.

33. Levring TB, Hansen AK, Nielsen BL, et al. Activated human CD4+ T cells express transporters for both cysteine and cystine. *Sci Rep.* 2012;2:266.

34. Siska PJ, Kim B, Ji X, et al. Fluorescence-based measurement of cystine uptake through xct shows requirement for ros detoxification in activated lymphocytes. *J Immunol Methods.* 2016;438:51-58.

35. Balkwill FR, Capasso M, Hagemann T. The tumor microenvironment at a glance. *J Cell Sci.* 2012;125:5591.

36. Merckx E, Albertini G, Paterka M, et al. Absence of system x(c)(−) on immune cells invading the central nervous system alleviates experimental autoimmune encephalitis. *J Neuroinflammation.* 2017;14:9.

FIGURES

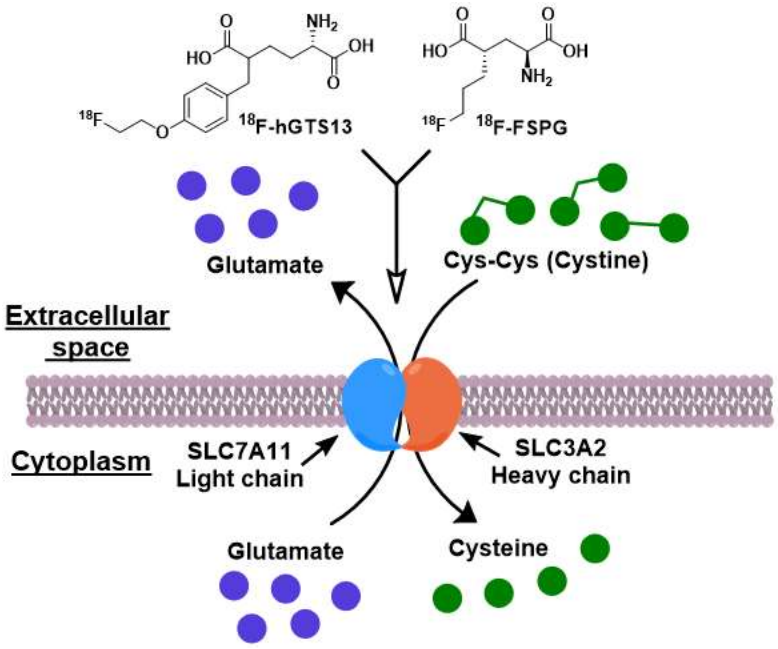

FIGURE 1*:* Graphical representation of system x_C^-, comprised of the heavy chain (SLC3A2) and light (SLC7A11) chain, x_C transporter, coupled by a disulfide bond (S-S). x_C^- imports extracellular cystine in exchange for intracellular glutamate in a 1:1 ratio. 18F-hGTS13 and 18F-FSPG bear structural similarities to glutamate and are transported into the cell via x_C^-.

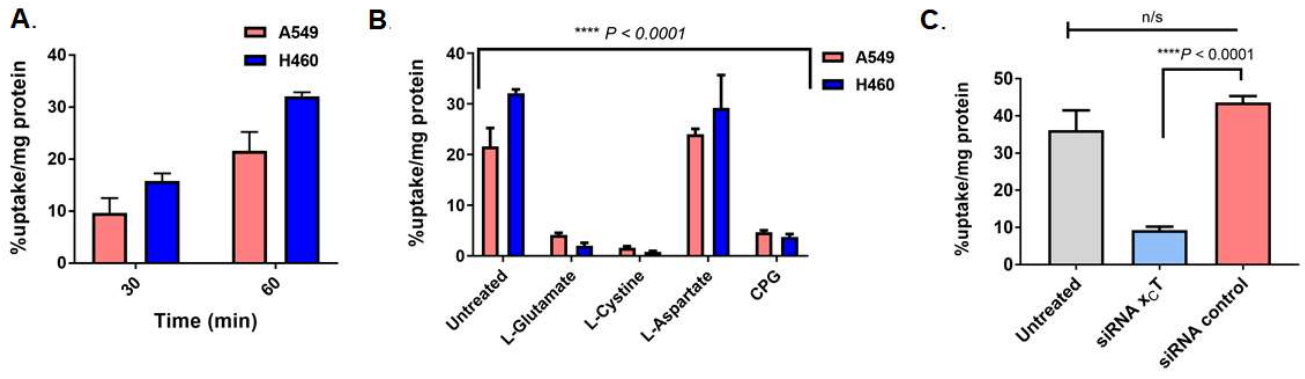

FIGURE 2: A. Cellular uptake of 18F-hGTS13 over time in A549 and H460 lung carcinoma cell lines. **B**. Competition studies of 18F-hGTS13 in A549 and H460 cells at 60 min post addition of radioactivity. There was a significant interaction on the inhibitor and cell line (****, $p<0.0001$, n=3 per condition). In A549 and H460 cells, 18F-hGTS13 uptake was significantly reduced in L-Glutamate treated cells ($p<0.0001$ for both cell lines, A549 81% decrease, H460 94% decrease), L-Cystine treated cells ($p<0.0001$ for both cell lines, A549 93% decrease, H460 97% decrease), CPG treated cells ($p<0.0001$ for both cell lines, A549 78% decrease, H460 88% decrease), a non-significant reduction was observed in L-Aspartate treated cells ($p=0.74$ in A549 cells, $p=0.59$ for H460 cells). CPG, (*S*)-4-carboxylphenylglycine. **C**. Reduced 18F-hGTS13 uptake was evident in A549 cells treated with x_CT siRNA compared to control siRNA ($p<0.0001$, n=3 per condition). No difference in uptake was evident in untreated cells compared to control siRNA ($p=0.10$, n=3 per condition).

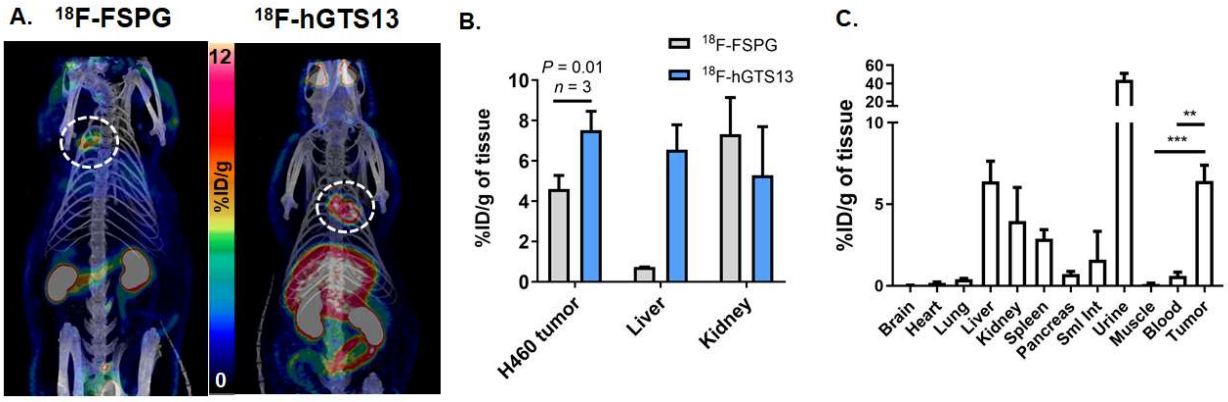

FIGURE 3*:* **A**. Representative maximum intensity projections (MIP) PET/CT images of rats bearing subcutaneous H460 tumors 60 min post intravenous administration of ~15 MBq of 18F-FSPG or 18F-hGTS13. **B**. Levels of radioactivity in H460 tumors at 60 mins post injection of radioactivity with 18F-FSPG and 18F-hGTS13 (p=0.01, n=3) and in liver and kidneys determined from PET imaging. **C**. *Ex vivo* biodistribution at ~80 mins post injection of 18F-hGTS13, n=3 animals, **p=0.0042, ***p=0.0004. K, kidney; Liv, liver; P, pancreas; Sml. Int., small intestine.

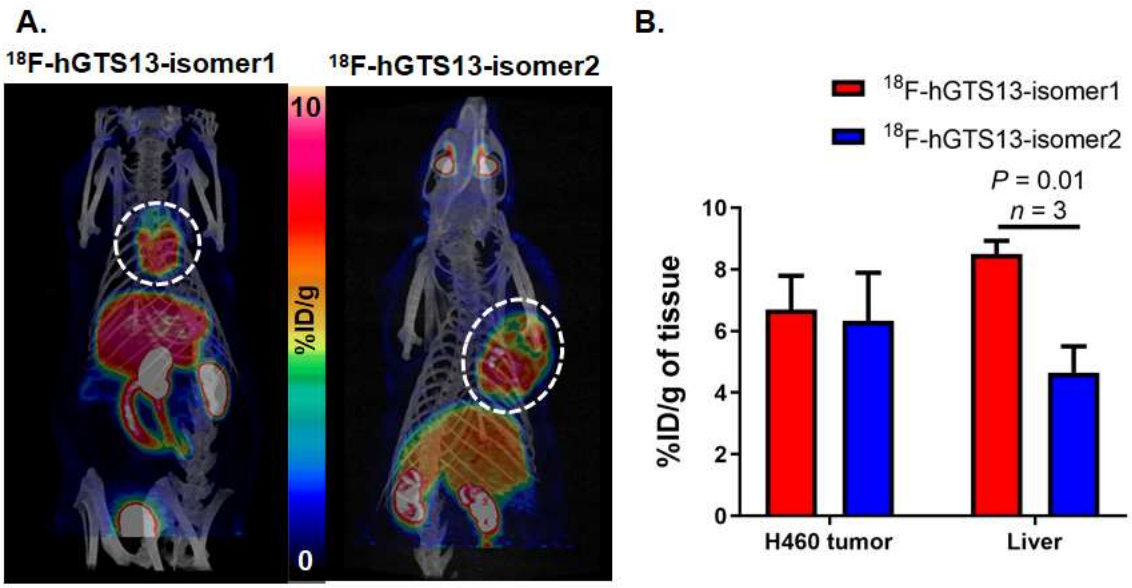

FIGURE 4: A. Representative MIP PET/CT images at 60 min post tail-vein injection of ~15 MBq of 18F-hGTS13-isomer1 or 18F-hGTS13-isomer2 in H460 tumor bearing rats. **B**. Levels of radioactivity retained in H460 tumors and liver (p=0.01, n=3).

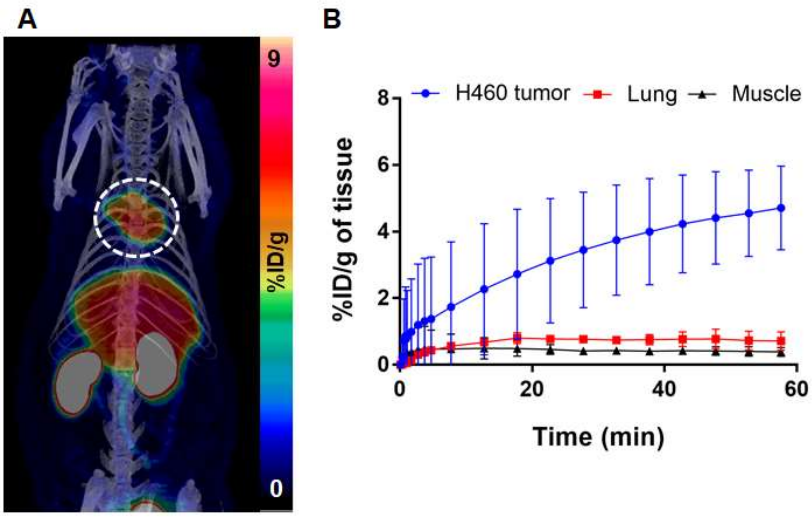

FIGURE 5: A. Representative summed 25-60 min MIP PET/CT image of H460 tumor bearing rat. **B**. Time activity curves reflecting 18F-hGTS13-isomer2 tumor uptake

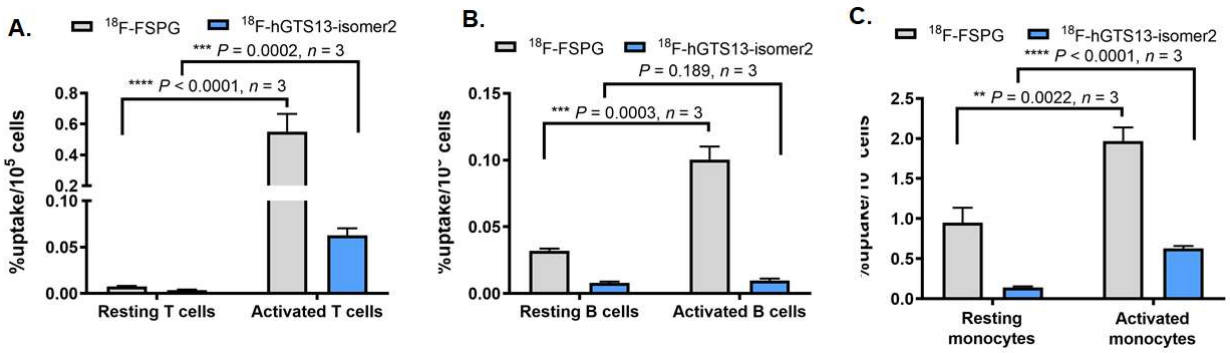

FIGURE 6*:* Cellular uptake of 18F-FSPG and 18F-hGTS13-isomer2 in resting and activated human **A**. T cells (18F-FSPG resting vs activated, p<0.0001, n=3; 18F-hGTS13-isomer2 resting vs activated, p=0.0002, n=3), **B**. B cells (18F-FSPG resting vs activated, p=0.0003, n=3; 18F-hGTS13-isomer2 resting vs activated, p=0.189, n=3), and **C**. monocytes (18F-FSPG resting vs activated, p=0.0022, n=3; 18F-hGTS13-isomer2 resting vs activated, p<0.0001, n=3).

SUPPLEMENTAL MATERIAL.

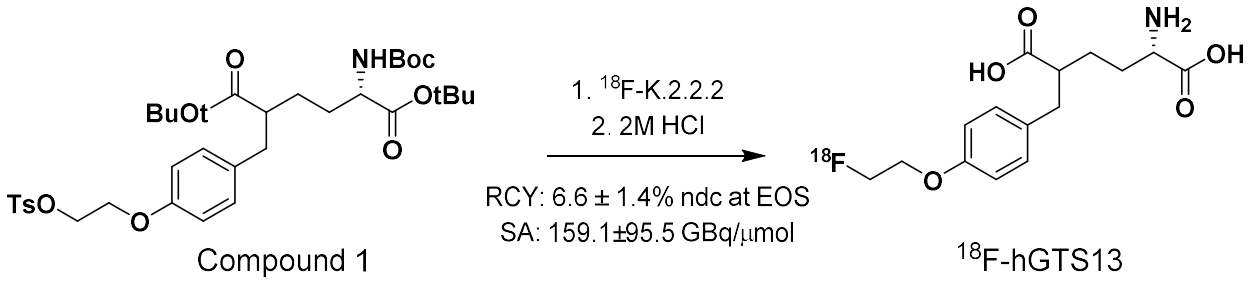

Supplemental Figure 1. Radiosynthesis of 18F-hGTS13. 18F-hGTS13 is synthesized via a two-step method from the corresponding protected, tosylate precursor (compound 1). RCY, radiochemical yield; ndc, non-decay corrected; SA, specific activity.

Radiosynthesis of 18F-hGTS13

No carrier added-aqueous [^{18}F]fluoride ion was produced on a PETtrace 880 cyclotron (GE Healthcare, USA) by irradiation of 2.0 mL water target using a 16 MeV proton beam on 99% enriched 18O-H_2O by the [18O(p,n)18F] nuclear reaction. 18F-Fluoride ion in [^{18}O]H_2O was transferred to a GE TRACERlab FXFN synthesizer and trapped on an anion exchange resin (QMA cartridge). Radioactivity was eluted with K_2CO_3/K222 solution (acetonitrile/water) into the reaction vial. Azeotropic drying was completed at 65 ˚C under helium flow and vacuum, followed by heating at 88 ˚C under vacuum. The precursor, (compound 1, 0.5-1.0 mg) in 1 mL anhydrous acetonitrile was added to the dried residue and the resulting mixture heated for 10 minutes at 100 ˚C. After cooling to 40 ˚C, 2M HCl (1 mL) was added and the mixture heated at 120 ˚C for 10 minutes. The crude product was diluted with acidified water (pH 2, 30 mL) and passed through a preconditioned Strata-X-C cartridge (Phenomenex, Torrance, CA). The cartridge was washed with 30 mL acidified water (pH 2) and 15 mL ethanol. The crude product was then eluted with 4 mL

phosphate buffer (7 g $Na_2HPO_4 \cdot 2H_2O$; 6 g NaCl in 1 L water) and injected onto a high performance liquid chromatography Phenomenex Gemini C-18, 5 µm (10 mm × 250 mm) semi-preparative reversed-phase column. A mobile phase of H_2O (0.1% TFA)/ acetonitrile (0.1% TFA), was used with a flow rate of 3.0 mL/min, and the retention time (Rt) of 18F-hGTS13 was 14.5min. The radioactive peak corresponding to 18F-hGTS13 was diluted (H_2O, pH 2, 20 mL) and trapped on a preconditioned Strata-X-C cartridge. The product was eluted from the cartridge using phosphate buffer (5mL) and then transferred into a sterile 10 mL vial. The radiochemical yield was 6.6 ± 1.4% (non-decay corrected at end of synthesis (EOS)) with a molar activity of 159.1±95.5 GBq/µmol (4.3±2.6 Ci/µmol) (n=4) and chemical and radiochemical purity greater than 95%. The chemical and radiochemical purities were determined by analytical high performance liquid chromatography (Gemini C-18, 5µm, 4.6 mm × 250 mm, Phenomenex). A mobile phase of H_2O (0.1% TFA)/ acetonitrile (0.1% TFA), was used with a flow rate of 1.0 ml/min, and Rt of 18F-hGTS13 was 9.8 min. The identity of 18F-hGTS13 was confirmed through co-injection with 19F-hGTS13 (Supplemental Fig. 2).

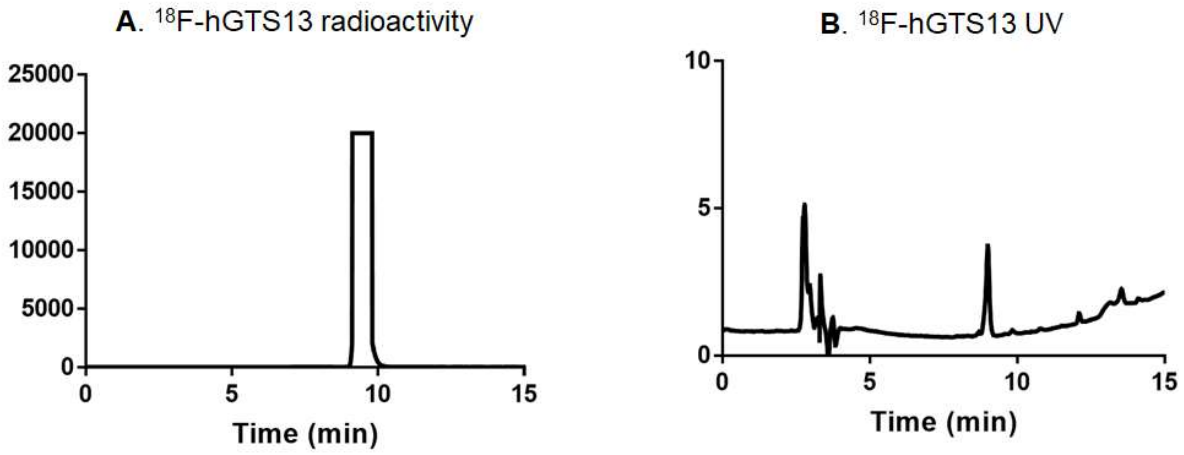

Supplemental Figure 2: Analytical profile of 18F-hGTS13 including **A**. radioactivity and **B**. UV spectrum

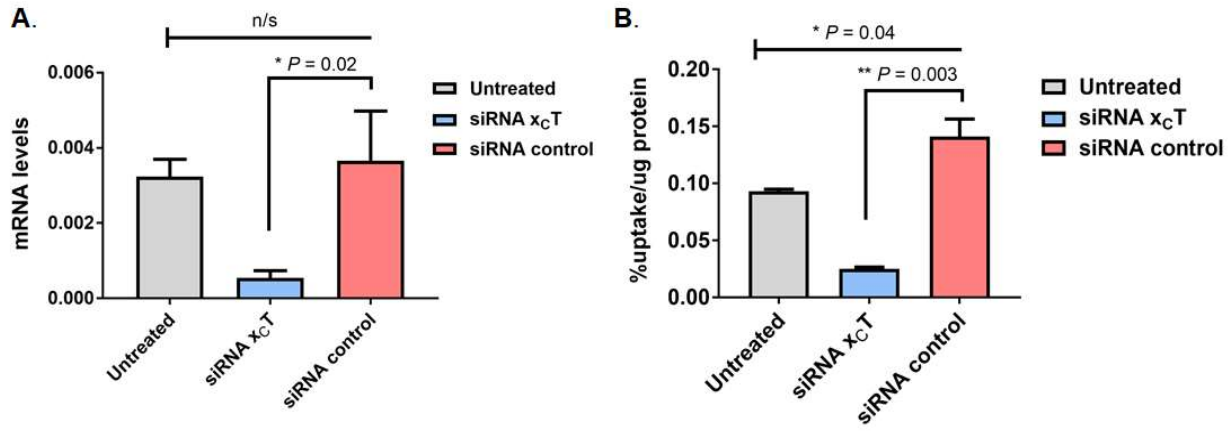

Supplemental Figure 3*:* **A**. mRNA levels of x_C^- in A549 cells treated with x_C^- siRNA, control siRNA and untreated cells (*p=0.02, n=3 per condition). No significant difference was found between untreated cells and cells treated with control siRNA. **B**. 14C-cystine cellular uptake after modification of x_C^- expression in A549 cells. A significant reduction in uptake was seen in cells treated with x_C^- siRNA compared to cells treated with control siRNA (**p=0.009, n=3 per

condition). A slight increase in uptake was evident in cells treated control siRNA relative to untreated cells (p=0.04, n=3 per condition).

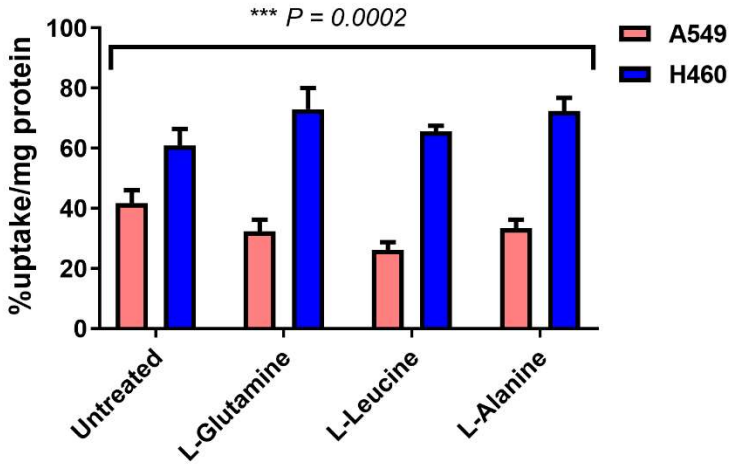

Supplemental Figure 4: Competition studies with 18F-hGTS13 in A549 and H460 cells are shown in the presence of L-Glutamine, L-Leucine and L-Alanine. There was a significant interaction on the class of inhibitor used and cell line studied (***, p=0.0002, n=4 per condition). In A549 cells, 18F-hGTS13 uptake was not significantly different in L-Glutamine or L-Alanine treated cells, however a significant reduction was observed in L-Leucine treated cells (***p=0.0003, 37% decrease). In H460 cells, 18F-hGTS13 uptake was not significantly different in L-Leucine treated cells, however a significant increase in radiotracer uptake was observed in L-Glutamine treated cells (**p=0.0053, 19% increase) and L-Alanine treated cells (**p=0.0085, 18% increase).

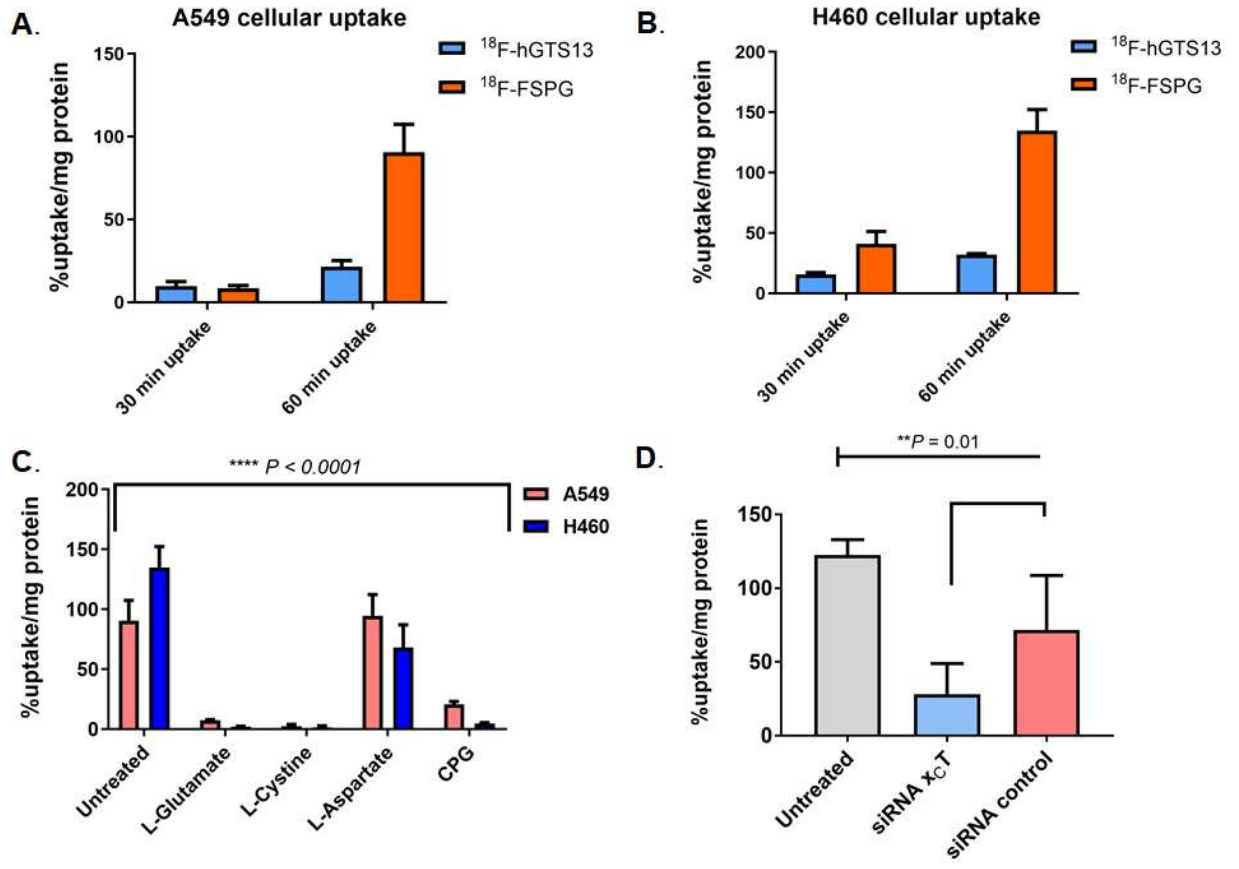

Supplemental Figure 5*:* Cell culture profile of 18F-FSPG and 18F-hGTS13 is shown over a 30 and 60 min time course in **A**. A549 and **B**. H460 cells. **C**. Competition studies with 18F-FSPG in A549 and H460 cells are shown in the presence of L-glutamate, L-cystine, L-aspartate and CPG. There was a significant interaction on the class of inhibitor used and cell line studied (****, $p<0.0001$, n=3 per condition). In the presence of L-Glutamate, A549 and H460 cells showed a 92 and 98% decrease in uptake respectively. In the presence of L-Cystine, A549 and H460 cells showed a 97 and 97% decrease in uptake respectively. In the presence of CPG, A549 and H460 cells showed a 77 and 96% decrease in uptake respectively. **D**. Specificity of 18F-FSPG to measure x_C^- in A549 cells, 18F-FSPG cellular uptake in A549 cells is shown after modification of x_CT expression, n=3 per condition. CPG, (*S*)-4-carboxylphenylglycine. A significant reduction in cellular uptake was observed in cells treated with x_CT siRNA compared to control siRNA

(*p=0.03, n=3 per condition), a significant reduction in radiotracer uptake was also observed between untreated cells and cells treated with control siRNA (**p=0.01, n=3 per condition).

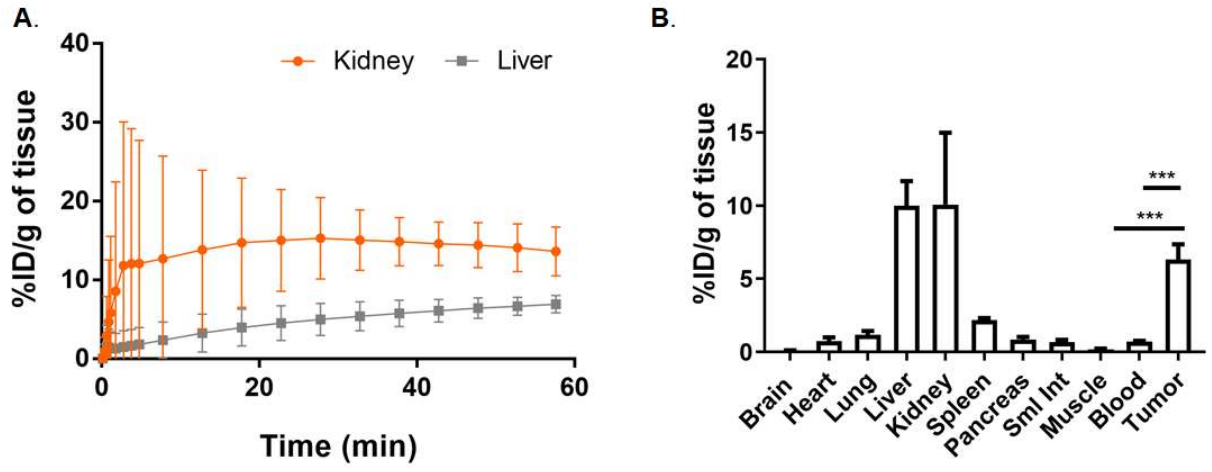

Supplemental Figure 6: A. Time activity curves reflecting 18F-hGTS13-isomer2 excretion profile. **B**. *Ex vivo* biodistribution of H460 tumor bearing rats after the completion of dynamic PET/CT scans, ~80 min post injection of radioactivity. Tumor-to-muscle, ***p=0.0006; tumor-to-blood, ***p=0.0008, n=3 per condition.